Materials and Design 54 (2014) 137–143

Contents lists available at ScienceDirect

Materials and Design

journal homepage: www.elsevier.com/locate/matdes

Technical Report

Influence of laser dispersed treatment on rolling contact wear and fatigue behavior of **railway** wheel steel

Dongfang Zeng [a], Liantao Lu [a,*], Zhengyang Li [b], Jiwang Zhang [a], Xuesong Jin [a], Minhao Zhu [a]

[a] State Key Laboratory of Traction Power, Southwest Jiaotong University, Chengdu 610031, China
[b] Institute of Mechanics, Chinese Academy of Sciences, Beijing 100190, China

ARTICLE INFO

Article history:
Received 6 May 2013
Accepted 11 August 2013
Available online 21 August 2013

ABSTRACT

The aim of this paper is to improve the rolling contact wear and fatigue resistance of ferrite–pearlite **railway** wheel steel by laser dispersed treatment. Such treatment creates isolated glazed regions on the surface layer of **railway** wheel steel, which are composed of fine martensite and retained austenite and have an average hardness of $762HV_{0.3}$. The wear rate and rolling contact fatigue life of treated and untreated **railway** wheel steel were evaluated and compared by Amsler twin-disc testing machines in dry and lubricated condition, respectively. The test results show that laser dispersed treatment improves the rolling contact wear and fatigue resistance of **railway** wheel steel. The stable wear rate of the laser treated **railway** wheel steel is about 0.3 times that of untreated **railway** wheel steel and the average rolling contact life of treated **railway** wheel steel is about double that of the untreated steel. Further investigations show that the glazed regions suppress the plastic deformation of **railway** wheel steel. This inhibits the treated **railway** wheel steel from delamination wear and delays the formation of fatigue crack initiation.

1. Introduction

Ferrite–pearlite steel is the most widely used material for **railway** wheel. However, such **railway** wheel steel cannot meet the strict demands for rolling contact wear and fatigue resistance with the rising speed and weight of traffic. Recently a series of laser surface treatment technologies, such as laser hardening, laser melting and laser cladding of wheel/rail have been applied for improving rolling contact wear and fatigue resistance of wheel/rail [1–3]. Because the size of the laser beam is small, it is necessary to scan the laser beam in order to obtain a large hardened area. In this case, multiple overlapping laser tracks are indispensable when a large area is required to be treated [4–6]. The formation of soft zones caused by tempering effect and low compressive residual stresses in the overlapping tracks are reported to produce a long narrow crack along the edge of the overlapping tracks and cause premature failure [4,5,7,8]. So it is considered that laser dispersed treatment (LDT), which creates isolated laser hardening spots in a certain pattern on a component surface, is an appropriate treatment for resolving the above problem. Compared with the conventional laser surface treatment technologies, the multiple overlapping laser tracks that cause the premature failure are avoided by LDT [9,10].

However, the investigation of influence of LDT on rolling contact wear and fatigue behavior of **railway** wheel steel had not been conducted. Then, in this study, the rolling contact wear and fatigue tests were conducted using treated and untreated **railway** wheel steel in order to clarify the influence of LDT on rolling contact wear and fatigue behavior of ferrite–pearlite **railway** wheel steel. In addition, based on X-ray diffraction (XRD) analysis, microhardness measurement, microstructures and worn surfaces observation, the effects of the microstructures resulted from LDT on wear mechanism and rolling contact fatigue (RCF) resistance were discussed.

2. Experimental procedure

2.1. Materials

Wheel and rail test discs were cut from **railway** wheel rim and railhead. Discs were machined into the shapes shown in Fig. 1. In order to ensure the uniformity of properties, wheel and rail discs were cut with their top surfaces parallel and close to the **railway** wheel tread and the top surface of railhead, respectively. The chemical compositions and hardness of the materials are given in Table 1.

LDT on the surface of wheel discs was performed using a pulse YAG laser set under an argon gas shield. The diameter of laser beam was 1 mm and the duration of laser pulse was 10 ms. The pulse energy of a single laser was about 9 J. Fig. 2 shows the photograph of treated wheel discs. LDT created isolated laser hardening spots on the surface of wheel disc which were selected to cover the whole surface without spots overlapping. Before the

* Corresponding author. Tel.: +86 28 86466025; fax: +86 28 87600868.
E-mail address: luliantao@swjtu.cn (L. Lu).

0261-3069/$ - see front matter © 2013 Elsevier Ltd. All rights reserved.
http://dx.doi.org/10.1016/j.matdes.2013.08.041

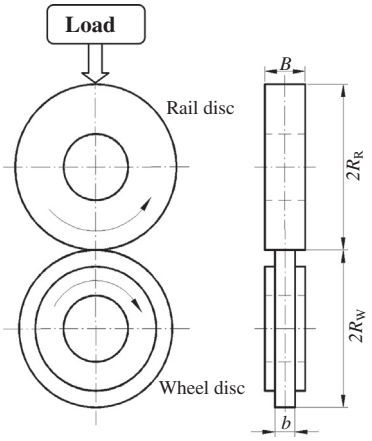

Fig. 1. Shapes of test discs and schematic illustration of wear and RCF tests.

wear and RCF tests, both treated and untreated discs were grounded to make the surface roughness of about 0.4 μm.

Both treated and untreated discs were sectioned, mounted, grounded, polished and etched with 2% nital solution. The microstructures were observed using a scanning electron microscopy (SEM). The phase structures were analyzed by XRD. The hardness was measured by a Vickers microhardness tester.

2.2. Rolling contact wear tests

Rolling contact wear tests were carried out with Amsler twin-disc rolling/sliding testing machines according to the Chinese standard GB 12444.1-90 [11]. The top disc was mounted in a swinging bracket to which load was applied by a compressed spring. This spring provided a load range of 0–2 kN. This machine could use the line contact between two cylindrical test discs to simulate the normal load and slip present at rail/wheel contact under dry condition. The schematic illustration of wear test is shown in Fig. 1.

The maximum Hertzian contact pressure in the line contact between the test discs is calculated using the equation quoted by Timoshenko and Goodier [12] for two elastically identical steel cylinder. Maximum Hertzian contact pressure is given by

$$p_0 = 0.418\sqrt{\frac{WE}{bR}} \tag{1}$$

where W is the contact load (N), b is the line contact length (mm), E is the modulus of elasticity of steel (MPa) and R is given by

$$\frac{1}{R} = \frac{1}{R_R} + \frac{1}{R_W} \tag{2}$$

where R_R and R_W (mm) are the radii of the rail (top) and wheel (bottom) disc, respectively.

The slip ratio (as a percentage) representing the ratio of sliding to rolling distances is defined as

$$g(\%) = 200 \times \frac{R_W n_W - R_R n_R}{R_W n_W + R_R n_R} \tag{3}$$

where R_R and R_W are as defined in Eq. (2), and n_R and n_w (rpm) are the speeds of the rail and wheel discs, respectively.

Table 1
Chemical compositions and hardnesses of the test materials.

Material	Compositions (%)						Microhardness ($HV_{0.3}$)
	C	Si	Mn	P	S	Cr	
Wheel steel	0.57	0.26	0.73	0.007	0.002	0.26	281
Rail steel	0.71	0.25	1.41	⩽0.03	⩽0.03		285

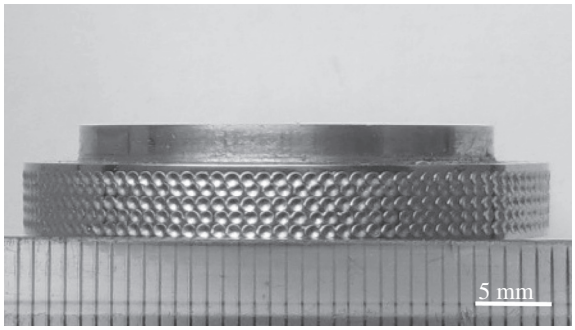

Fig. 2. Photograph of the treated wheel discs before being grounded.

All wear tests were conducted under a maximum contact pressure of 800 MPa and a slip ratio of 5.4% to simulate the wearing condition in curved tracks. During tests the contact area was cooled with compressed air to prevent the change of the microstructure by heating and to remove wear debris. Dimensions of wear test discs and wear test conditions are given in Table 2.

The tests were performed for 100,000 cycles on both treated and untreated discs. The tests were stopped every 10,000 cycles to measure weight losses by an electronic balance with a sensitivity of ±0.1 mg. Then, the discs were remounted in the wear machine at the same location. At the end of each test, discs were sectioned along the track center and prepared for metallographic observation using optical microscopy (OM) and SEM. The microstructures of worn surfaces were observed by SEM to analyze the wear mechanism.

2.3. RCF tests

RCF tests were carried out on another Amsler twin-disc rolling/sliding testing machine according to the Chinese standard GB 10622-89 [13]. The normal load was applied by a hydraulic piston which provided a load range of 0–30 kN. The schematic illustration of RCF test is shown in Fig. 1.

At all times throughout a test the contact area between two discs was lubricated by machine oil SEA 20. The volume of machine oil was 1 L/min. A counter recorded the number of revolutions. The criterion for the end of RCF life involved either the loss of surface material as spalling or a collapse of the fatigue damaged surface. Both cases led to an increase in the vibration level detected by an accelerometer mounted on the machine. When the vibration reached the preset value the accelerometer activated a cut-off switch and the test stopped. RCF life was reported as the number of revolutions and involved crack initiation and growth.

All tests were conducted under a maximum contact pressure of 1500 MPa and a slip ratio of −5.1%. Dimensions of RCF test discs and RCF test conditions are given in Table 2. At the end of each test, metallographic observation was performed as mentioned above and the RCF damage surface morphologies were observed by SEM.

3. Results

3.1. Microstructures and hardness

Fig. 3a shows the microstructure of **railway** wheel steel used in this study. The microstructure of the **railway** wheel steel is composed of ferrite and pearlite, which has an average hardness of 281$HV_{0.3}$. The cross-sectional SEM micrograph of the treated wheel disc is shown in Fig. 3b. Two different regions are presented in the surface layer, i.e. untreated substrate regions and glazed regions. The depth and width of the glazed regions are around 610 μm

Table 2
Dimensions of test discs and test conditions.

Test conditions	Wear tests	RCF tests
Disc dimension/mm		
Wheel disc	$b = 5$, $R_W = 19$	$b = 5$, $R_W = 30$
Rail disc	$B = 10$, $R_R = 20$	$B = 10$, $R_R = 30$
Test speed/rpm		
Wheel disc	200	950
Rail disc	180	1000
Normal load/N	876	4744
Maximum contact pressure/MPa	800	1500
Slip ratio/%	5.4	−5.1
Test environment	Dry, air cooled	Oil lubricated

and 970 μm, respectively. The high magnification microstructure of region A, as shown in Fig. 3c, indicates the intimately bonded interface between untreated substrate region and glazed region. The microstructure of glazed region is mainly composed of fine martensite due to high solidification rates experienced during laser processing [2,3], as shown in Fig. 3d. The glazed regions have an average hardness of $762HV_{0.3}$.

The XRD pattern of the surface of treated wheel disc, shown in Fig. 4, confirms that the main phase in the glazed region is martensite. The XRD pattern also indicates that the glazed region also contains a small amount of retained austenite. Shariff et al. stated that the microstructure of laser treated pearlite steel was composed of martensite and austenite [14]. The microstructure of laser treated region was determined not only by chemical and phase composition of the treated materials, but also by laser processing, such as power density, scanning speed and diameter of laser beam. In this case, the power density of laser beam and laser irradiation duration used are 10^5 W/cm^2 and 10 ms, respectively, which are similar to that of laser beam used in Ref. [8]. Therefore the amount of retained austenite in the glazed region can be conjectured as no more than 10%, which are similar to the amount of retained austenite reported in Ref. [8]. After treatment, it can be seen that the intensity peaks are obviously reduced and the width of diffraction peaks becomes broadened. This indicates the existence of refined grain [15,16], arising from rapid solidification of the melt due to high cooling rates experienced in laser process, which can increase the hardness of the glazed regions.

3.2. Wear test result

3.2.1. Wear rate

Measuring the weight loss of the wheel discs at regular intervals of 10,000 cycles enabled the wear behavior to be monitored as rolling/sliding proceeds. Wear rate (weight loss per meter) of wheel disc is plotted in Fig. 5 against number of rolling cycles. It can be seen that the wear rate of the untreated wheel disc increases with number of rolling cycles until around 30,000∼40,000 cycles, where the maximum and stable wear rate is reached for the remainder of the test. The wear rate of treated wheel disc reaches the maximum at around 10,000 cycles, thereafter decreasing with number of rolling cycles until around 20,000 cycles, where the stable wear rate is reached for the remainder of the test. Based on the observation of worn surface (see Fig. 6), it can be seen that the substrate with low hardness would be worn away first, which leads to high wear rate during the first 10,000 cycles and the raising of glazed regions. Because the substrate is being worn away, more and more loads would be carried by the glazed regions with high hardness, which leads to the decreasing of wear rate during 10,000–20,000 cycles. During 20,000–100,000 cycles, most of the substrate on the contact area has been worn away, so almost all the loads would be carried by glazed region, which leads to a stable wear rate. The stable wear rate of the laser treated wheel disc is superior, at about 0.3 times that of untreated wheel disc. Namely, LDT effectively improves the wear resistance of **railway** wheel steel.

3.2.2. Wear behavior

Fig. 6a is a SEM micrograph of worn surface of untreated wheel disc at the end of wear test, in which thin metallic flakes and pitting failures are formed on the surface the disc. Cross-sectional microstructure of untreated wheel disc is shown in Fig. 7a. It can be seen that the present loading has resulted in a large amount of plastic deformation below the wear surface of untreated disc

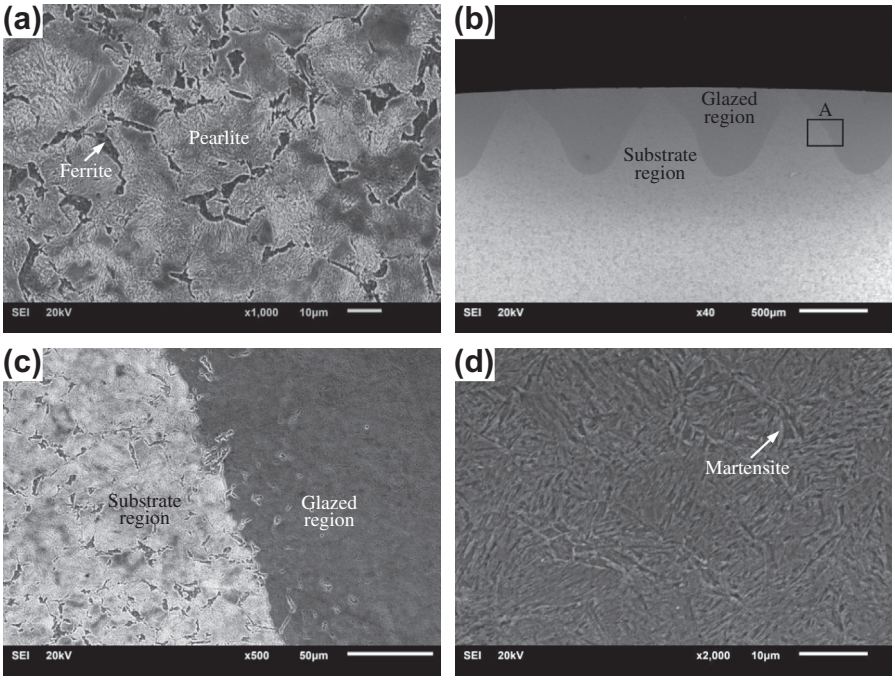

Fig. 3. SEM micrographs of (a) untreated wheel steel, (b) surface layer of treated wheel disc, (c) interface (region A) between untreated substrate region and glazed region, and (d) glazed region.

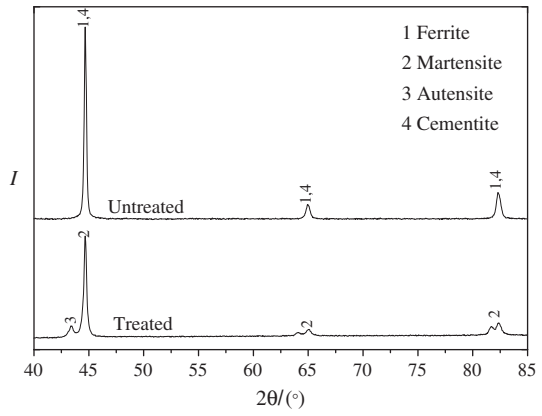

Fig. 4. XRD pattern of wheel discs.

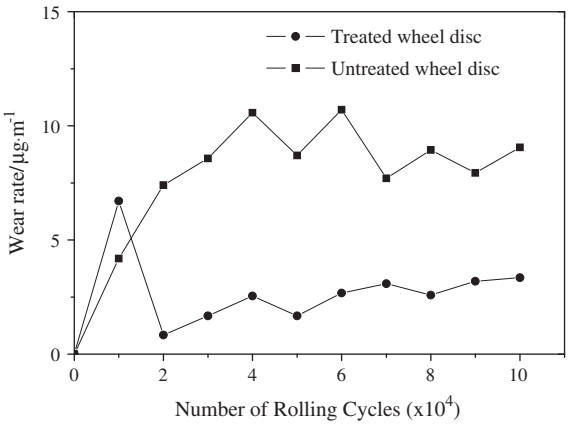

Fig. 5. Relationship between the wear rate of wheel discs and number of rolling cycles.

and the visible depth of deformation is about 100 μm. Crack initiation location is at the surface. Then crack propagation generally follows the direction of maximum strain, which induces the formation of metallic tongue on the surface. These metallic tongues are considered to be the origins of the thin metallic flakes observed in Fig. 6a. The thin metallic flakes and large plastic deformation below the surface confirm that the delamination is the dominant wear mechanism in the untreated disc, while the small size of pitting failure indicates that a slight fatigue wear mechanism is occurring.

Fig. 6b is a SEM micrograph of worn surface of treated wheel disc at the end of wear test. Compared to the untreated disc, the flake size is smaller and the pitting failure size is lager. Compared with glazed regions, more and lager particles are torn away from the surface of untreated substrate regions between the glazed regions. Cross-sectional microstructures of untreated substrate region and glazed region of treated wheel disc are shown in Fig. 7b and c, respectively. It can be seen that the visible depth of deformation of substrate region is about 10 μm, which is much shallower than that of untreated wheel disc (Fig. 7a). In addition, no obvious plastic deformation layer is found below the wear surface of glazed region. After LDT, the wear mechanism of the wheel discs alters and the main wear mechanism is fatigue wear, which is accompanied by slight delamination wear.

3.3. RCF test result

3.3.1. RCF lives

RCF lives of the treated and untreated wheel discs are shown in Table 3. It can be seen that the average RCF life of treated wheel discs is about double that of the untreated disc. This indicates that RCF resistance of **railway** wheel steel can be markedly improved by LDT.

3.3.2. RCF behavior

A phenomenon of macro-pitting is found on the surface of both treated and untreated wheel discs, as shown in Fig. 8. The arrowhead appearance of the pits suggests [17] that the phenomenon which occurred is the so-called "point surface origin macro-pitting": cracks start randomly at or very near the contact surface and then develop in a fanned-out appearance. Fig. 9 shows a RCF defect on the surface of treated wheel disc that haven't developed into a macro-pitting. It can be seen that the crack starts at the untreated substrate region.

The friction coefficients obtained in RCF tests for both treated and untreated discs are approximately 0.07. Contact theory predicts that such low friction coefficient values produce a position of maximum shear stress at the subsurface [18]. The maximum shear stress produces a layer of maximum plastic deformation at the subsurface of the untreated wheel disc, as shown in Fig. 10a and c. In addition to this subsurface deformation, the plastic deformation on the surface is also observed, which is shallow, approximately 10 μm deep, as shown in Fig. 10a and b. The layer of deformation is not observed at the subsurface of the treated wheel disc, as shown in Fig. 11a. A small amount of deformation is formed at the surface of substrate region (Fig. 11b), the lever of which is lower than that of untreated wheel disc (Fig. 10b). Besides, no plastic deformation is observed at the surface of glazed region, as shown in Fig. 11b.

4. Discussion

4.1. Influence of LDT on wear resistance

As stated above, the main wear mechanism of the untreated wheel disc is delamination. According to the delamination theory

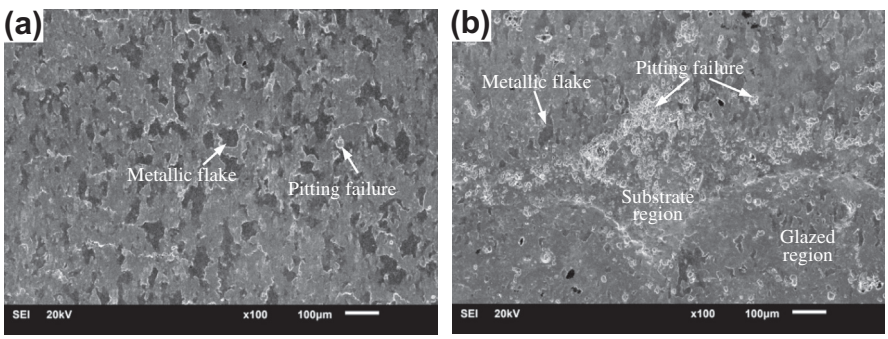

Fig. 6. SEM micrographs of worn surface of (a) untreated wheel disc and (b) treated wheel disc.

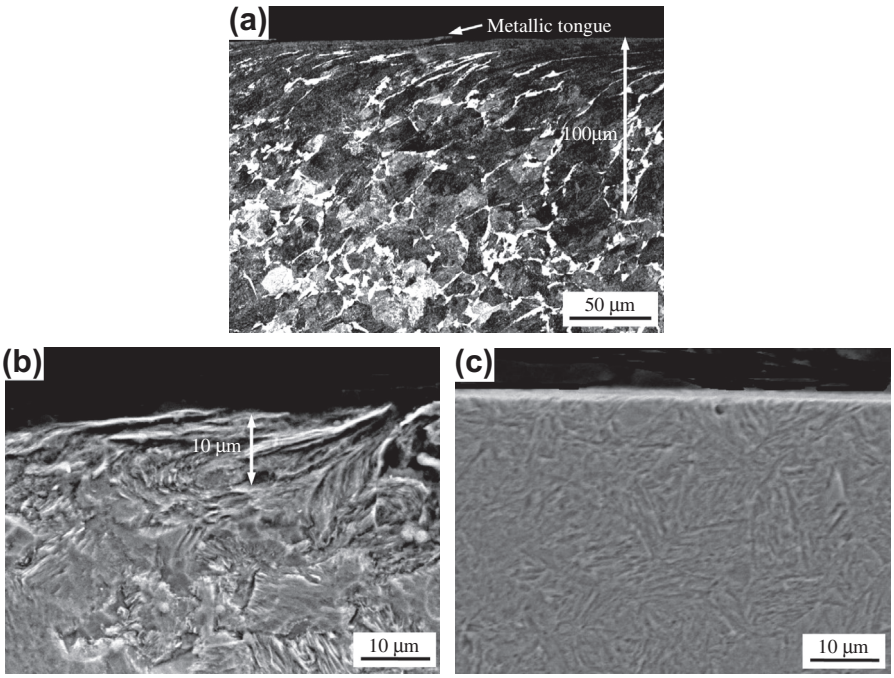

Fig. 7. Cross-sectional microstructures of (a) untreated wheel disc, (b) substrate region of treated wheel disc and (c) glazed region of treated wheel disc.

Table 3
RCF lives of treated and untreated wheel discs/cycles.

Wheel discs	No. 1	No. 2	Average
Untreated disc	145,201	150,240	147,721
Treated disc	289,512	305,421	297,467

of wear [19], the surface layer will accumulate plastic strain under rolling/sliding condition, which will lead to dislocation pile-up a finite distance from the surface and finally result in crack initiation on the surface. With accumulating of plastic strain, crack will propagate parallel to the wear surface. When this crack reaches a critical length, the material between the crack and the surface will shear, yielding a flake like particle. Hence, the resistance to delamination wear of **railway** wheel steel is dominated by the resistance to plastic deformation. Young et al. stated that during plastic deformation, the strength of the ductile phase is enhanced via plastic constraint by the surrounding stronger hard phase [20]. This structure in this case that the soft untreated substrate regions are surrounded by glazed regions with relatively higher hardness is similar. Because the plastic deformation of the substrate regions of treated disc is suppressed by the glazed regions, the plastic deformation depth of substrate region of treated disc (Fig. 7b) is much shallower than that of untreated wheel disc (Fig. 7a). This inhibits the substrate regions from delamination wear. The ferritic–pearlitic microstructure of substrate changes into fine martensite and retained austenite by LDT (Figs. 3 and 4). Such microstructures improve the plastic deformation resistance of the glazed regions by their higher hardness compared to untreated wheel disc. Consequently, no obvious plastic deformation layer is found below the wear surface of glazed region (Fig. 7c), which prevents the glazed regions from delamination wear. The higher hardness of the glazed regions is not only due to the martensite presented in the regions, but also the retained austenite which is strengthened by solid solution, dislocations and smaller grain size than that of conventional heat treatment [21]. The retained austenite is a metastable phase and some of which will change into strain induced martensite [16,22]. Colaco et al. claimed that strain induced transformation not only increases the effective hardness of the surface, but also dissipates energy, delaying the fracture process that causes material loss [23].

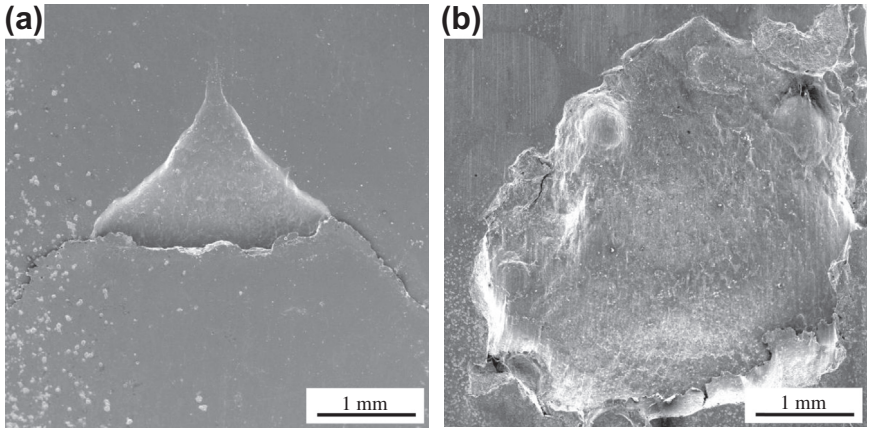

Fig. 8. Micrograph of macro-pitting RCF defect on the surface of (a) untreated wheel disc and (b) treated wheel disc.

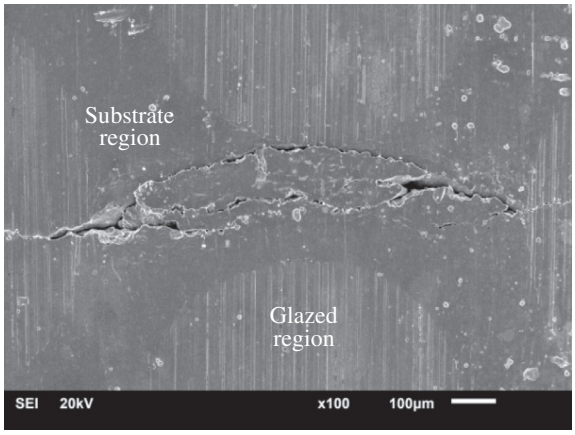

Fig. 9. A RCF defect that have not developed into a macro-pitting.

4.2. Influence of LDT on RCF resistance

For the **railway** wheel steel, the route to improve fatigue resistance is through delay of crack initiation since, once formed, cracks will grow rapidly in the presence of fluid. Crack formation in the wheel discs is preceded by a considerable amount of plastic deformation. The plastic deformation occurs both at the surface and subsurface of the untreated wheel disc (Fig. 10). However, as discussed above, cracks start at or very near the contact surface instead of the subsurface, the reason of which is that crack initiation at subsurface in the high strain region is inhibited by the compressed matrix and compressive residual stresses [24]. The glazed regions of treated wheel disc with a mixture of fine martensite and retained austenite have good resistance to plastic deformation. Therefore, no plastic deformation is observed at the glazed regions (Fig. 11), which inhibits crack initiation from the surface of glazed regions. Choi et al. also confirmed that the fine martensite is beneficial to resisting rolling contact fatigue [25]. Crack starts at the surface of substrate region after laser dispersed treatment (Fig. 9), since the plastic deformation is formed there (Fig. 11b). However, because the plastic deformation of the substrate regions is suppressed by the glazed regions, the lever of deformation of substrate region is much slower than that of untreated wheel disc (Fig. 10b). Therefore, the crack initiation from the substrate regions of treated disc is delayed, which prolongs the rolling contact life of treated wheel disc. Another reason for LDT to enhance RCF resistance is that the growth rate of cracks which start from the substrate region will decrease rapidly near the boundary between the substrate and glazed region [26,27].

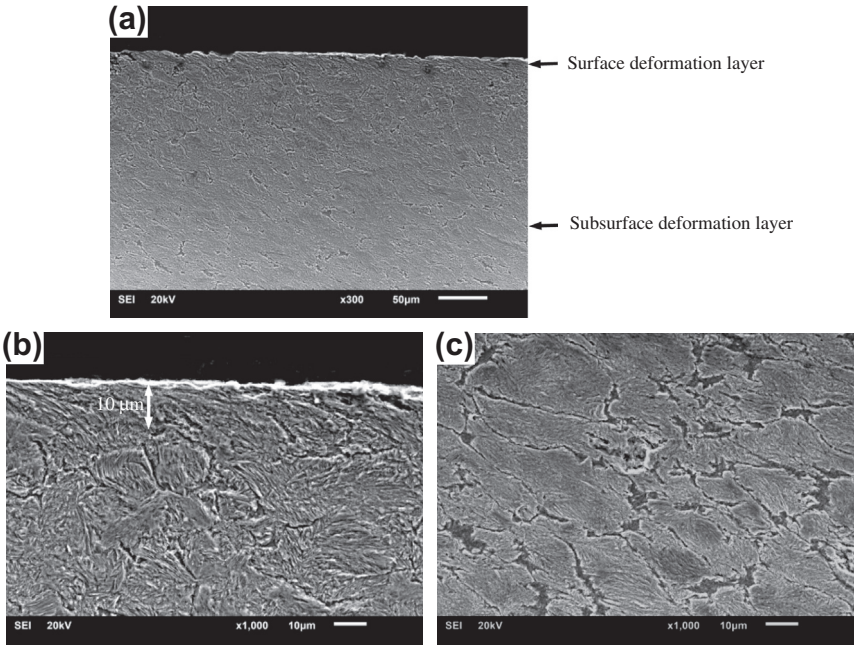

Fig. 10. Cross-sectional microstructures of (a) untreated wheel disc, (b) surface deformation layer and (c) subsurface deformation layer.

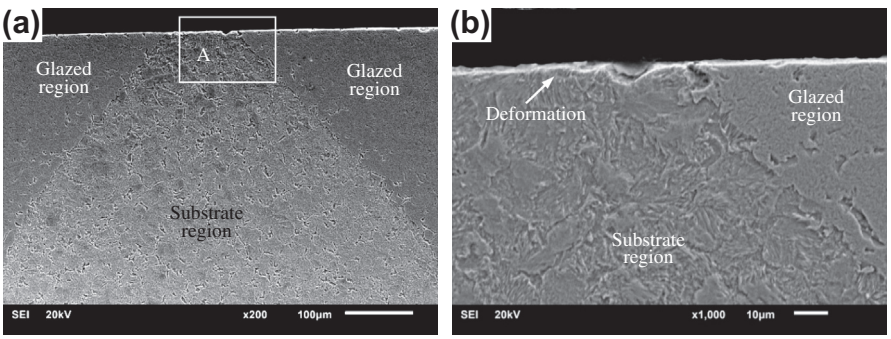

Fig. 11. Cross-sectional microstructures of (a) treated wheel disc and (b) surface (region A).

5. Conclusions

The following conclusions can be drawn from this investigation:

(1) LDT creates isolated glazed regions with an average hardness of 762$HV_{0.3}$ on the surface layer of **railway** wheel steel. The glazed regions are composed of fine martensite and retained austenite.
(2) LDT effectively improves both the wear resistance and RCF resistance of **railway** wheel steel. The stable wear rate of the laser treated wheel disc is about 0.3 times that of untreated wheel disc and the average RCF life of treated wheel discs is about double that of the untreated disc.
(3) The glazed regions suppress the plastic deformation. This inhibits the treated **railway** wheel steel from delamination wear and delays the formation of RCF crack initiation.

Acknowledgements

This work was supported by the National Key Technology R&D Program (2009BAG12A01-B10-1), Research and Development Program of the Ministry of Railway of China (2009J015) and Basic Research Association Foundation of High – speed Rail (U 1134202).

References

[1] Franklin F, Weeda GJ, Kapoor A, Hiensch E. Rolling contact fatigue and wear behaviour of the infrastar two-material rail. Wear 2005;258:1048–54.
[2] DiMelfi R, Sanders P, Hunter B, Eastman J, Sawley K, Leong K, et al. Mitigation of subsurface crack propagation in railroad rails by laser surface modification. Surf Coat Technol 1998;106:30–43.
[3] Aldajah S, Ajayi OO, Fenske GR, Kumar S. Investigation of top of rail lubrication and laser glazing for improved railroad energy efficiency. J Tribol 2003;125:643–8.
[4] Iino Y, Shimoda K. Effect of overlap pass tempering on hardness and fatigue behaviour in laser heat treatment of carbon steel. J Mater Sci Lett 1987;6:1193–4.
[5] Wang H, Bergmann H. Rapid graphitization of a pulsed laser remelted ductile cast iron during multipass overlap melting. Metall Mater Trans A 1995;26:793–800.
[6] Lima M, Goldenstein H. Structure of laser remelted surface of cast irons. Surf Eng 2000;16:127–30.
[7] Van Brussel B, Hegge H, De Hosson JTM, Delhez R, De Keijser TH, Van der Pers N. Development of residual stress and surface cracks in laser treated low carbon steel. Scr Metall Mater 1991;25:779–84.
[8] Van Brussel B, De Hosson JTM. Residual stresses in the surface layer of laser-treated steels. Mater Sci Eng, A 1993;161:83–9.
[9] Jiang J, Xue L, Wang S. Discrete laser spot transformation hardening of AISI O1 tool steel using pulsed Nd: YAG laser. Surf Coat Technol 2011;205:5156–64.
[10] Xue L, Islam M, McGregor G. Dot matrix hardening of steels using a fiber optic coupled pulsed Nd: YAG laser. Mater Manuf Process 1999;14:53–65.
[11] GB 12444.1-90. Metallic materials-MM mode wear test. Standardization administration of the People's Republic of China; 1990.
[12] Timoshenko SP, Goodier J. Theory of elasticity. McGraw-Hill; 1970.
[13] GB 10622–89. Metallic materials-rolling contact fatigue test. Standardization administration of the People's Republic of China; 1989.
[14] Shariff S, Pal T, Padmanabham G, Joshi S. Sliding wear behaviour of laser surface modified pearlitic rail steel. Surf Eng 2010;26:199–208.
[15] Cui C, Hu J, Liu Y, Gao K, Guo Z. Formation of nano-crystalline and amorphous phases on the surface of stainless steel by Nd: YAG pulsed laser irradiation. Appl Surf Sci 2008;254:6779–82.
[16] Gui-Fang S, Yong-Kang Z, Chang-Sheng L, Kai-Yu L, Xing-Qi T, Peng L. Microstructure and wear resistance enhancement of cast steel rolls by laser surface alloying NiCr–Cr 3C 2. Mater Design 2010;31:2737–44.
[17] Hyde RS. Contact fatigue of hardened steel. ASM International, Member/Customer Service Center, Materials Park, OH 44073-0002, USA; 1996. p. 691–703.
[18] Donzella G, Faccoli M, Ghidini A, Mazzu A, Roberti R. The competitive role of wear and RCF in a rail steel. Eng Fract Mech 2005;72:287–308.
[19] Suh NP. The delamination theory of wear. Wear 1973;25:111–24.
[20] Young CH, Bhadeshia H. Strength of mixtures of bainite and martensite. Mater Sci Technol 1994;10:209–14.
[21] Vilar R, Colaço R, Almeida A. Laser surface treatment of tool steels. Opt Quant Electron 1995;27:1273–89.
[22] Dan W, Li S, Zhang W, Lin Z. The effect of strain-induced martensitic transformation on mechanical properties of TRIP steel. Mater Design 2008;29:604–12.
[23] Colaco R, Pina C, Vilar R. Influence of the processing conditions on the abrasive wear behaviour of a laser surface melted tool steel. Scripta Mater 1999;41:715–21.
[24] Garnham JE, Davis CL. The role of deformed rail microstructure on rolling contact fatigue initiation. Wear 2008;265:1363–72.
[25] Choi B-Y, Shin J-H, Bahng G-W, Yoon K-B. Metallographic study on rolling contact fatigue of 0.44% C–1.71% Mn induction-hardened bearing steels. Wear 1996;192:1–5.
[26] Doong J-L, Tan Y-H. Effect of laser surface alloying chromium onto AISI 1018 steel on the fatigue crack growth rate. Int J Fatigue 1989;11:239–47.
[27] Tan Y, Wu G, Yang JM, Pan T. Laser shock peening on fatigue crack growth behaviour of aluminium alloy. Fatigue Fract Eng Mater Struct 2004;27:649–56.